fluids

MDPI

Supplementary Materials

Similarities and Contrasts in Time-Mean Striated Surface Tracers in Pacific Eastern Boundary Upwelling Systems: The Role of Ocean Currents in their Generation

Ali Belmadani [1,2,*], Pierre-Amaël Auger [1,3,4], Nikolai Maximenko [5], Katherine Gomez [1,3,6] and Sophie Cravatte [7]

1 Department of Geophysics, University of Concepcion, Concepcion 4070386, Chile
2 Météo-France, Direction Interrégionale Antilles-Guyane, Fort-de-France 97200, Martinique, France
3 Millennium Institute of Oceanography (IMO), University of Concepcion, Concepcion 4070386, Chile; katherine.gomez@imo-chile.cl
4 University of Brest, CNRS, IRD, Ifremer, Laboratoire d'Océanographie Physique et Spatiale (LOPS), IUEM, Brest 29280, France; pierre-amael.auger@ird.fr.
5 International Pacific Research Center, School of Ocean and Earth Science and Technology, University of Hawaii at Manoa, Honolulu, HI 96822, USA; maximenk@hawaii.edu
6 School of Marine Sciences, Pontifical Catholic University of Valparaiso, Valparaiso 2340000, Chile
7 Laboratoire d'Etudes en Géophysique et Océanographie Spatiale, Université de Toulouse, CNES, CNRS, IRD, UPS, Toulouse 31400, France; sophie.cravatte@legos.obs-mip.fr
* Correspondence: ali.belmadani@meteo.fr

Citation: Belmadani, A.; Auger, P.-A.; Maximenko, N.; Gomez, K.; Cravatte, S. Similarities and Contrasts in Time-Mean Striated Surface Tracers in Pacific Eastern Boundary Upwelling Systems: The Role of Ocean Currents in their Generation. *Fluids* **2021**, *6*, 455. https://doi.org/10.3390/fluids6120455

Academic Editor: Pavel S. Berloff

Received: 6 June 2021
Accepted: 10 November 2021
Published: 15 December 2021

List of Figures and Tables

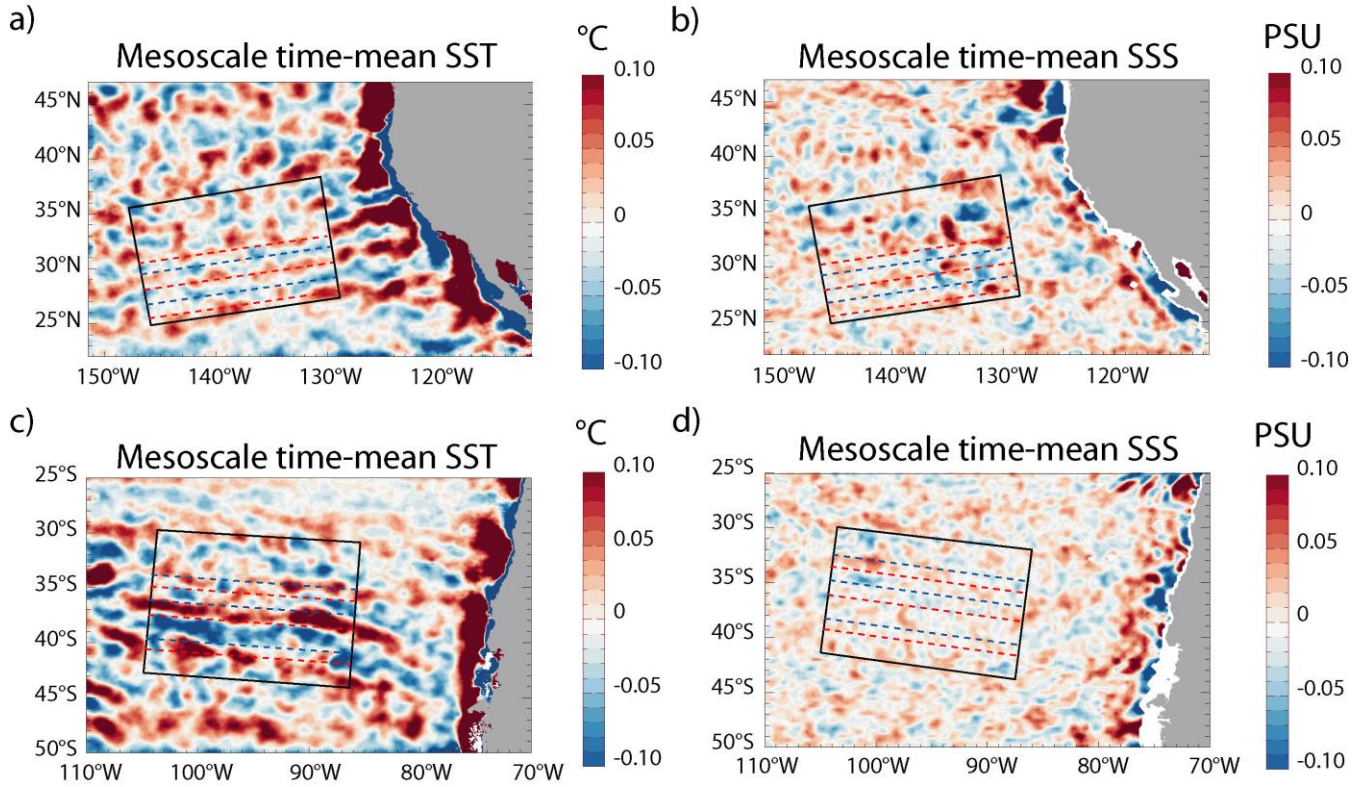

Figure S1. Striation expressions in hydrographical tracers in the two study regions from alternate data: (**a**,**b**) and (**c**,**d**) same as in Figures 2a,c and 3a,c, respectively, except for (**a**,**c**) OSTIA SST and (**b**,**d**) SMOS SSS. .

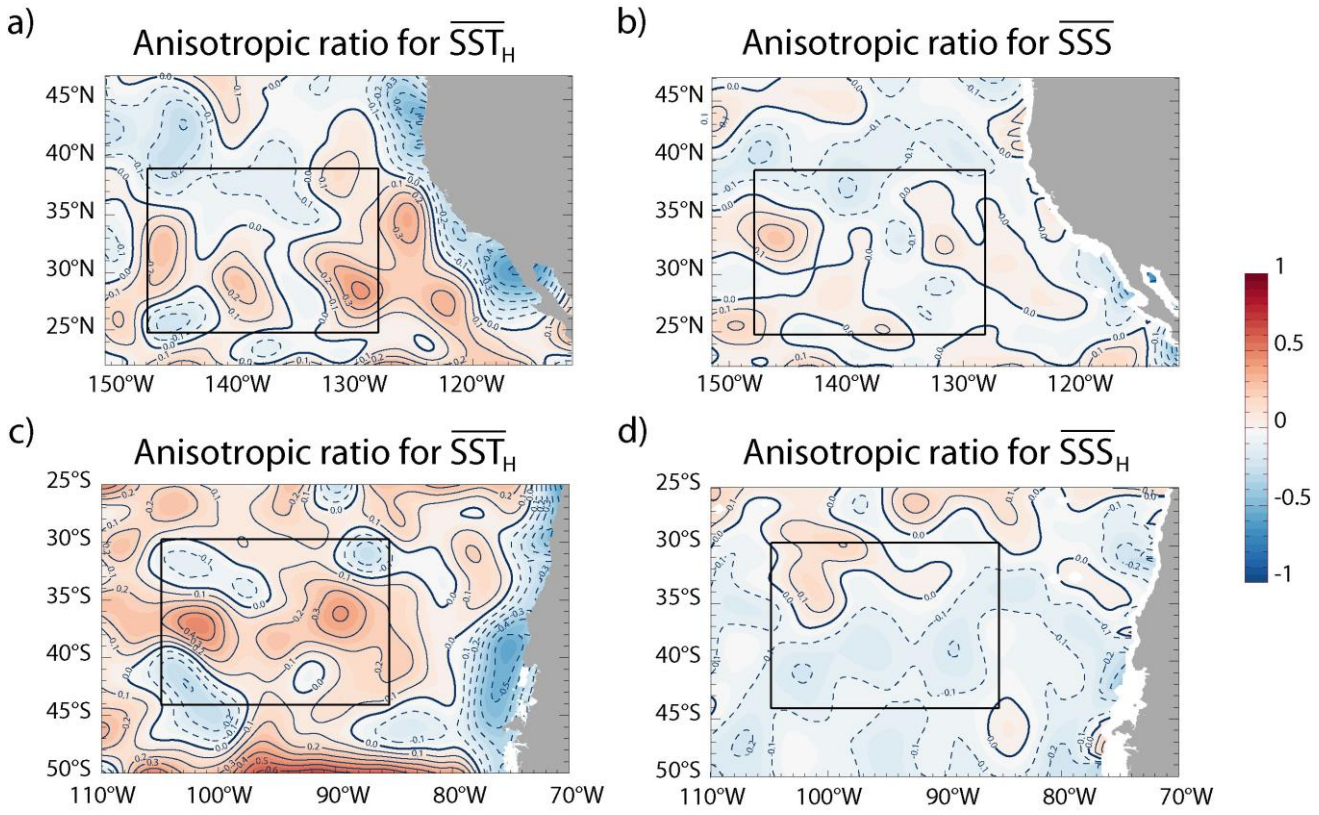

Figure S2. Anisotropic ratio for hydrographical tracers in the two study regions from alternate data: (**a**,**b**) and (**c**,**d**) same as in Figures B1a,b and B2a,b, respectively, except for (**a**,**c**) OSTIA SST and (**b**,**d**) SMOS SSS.

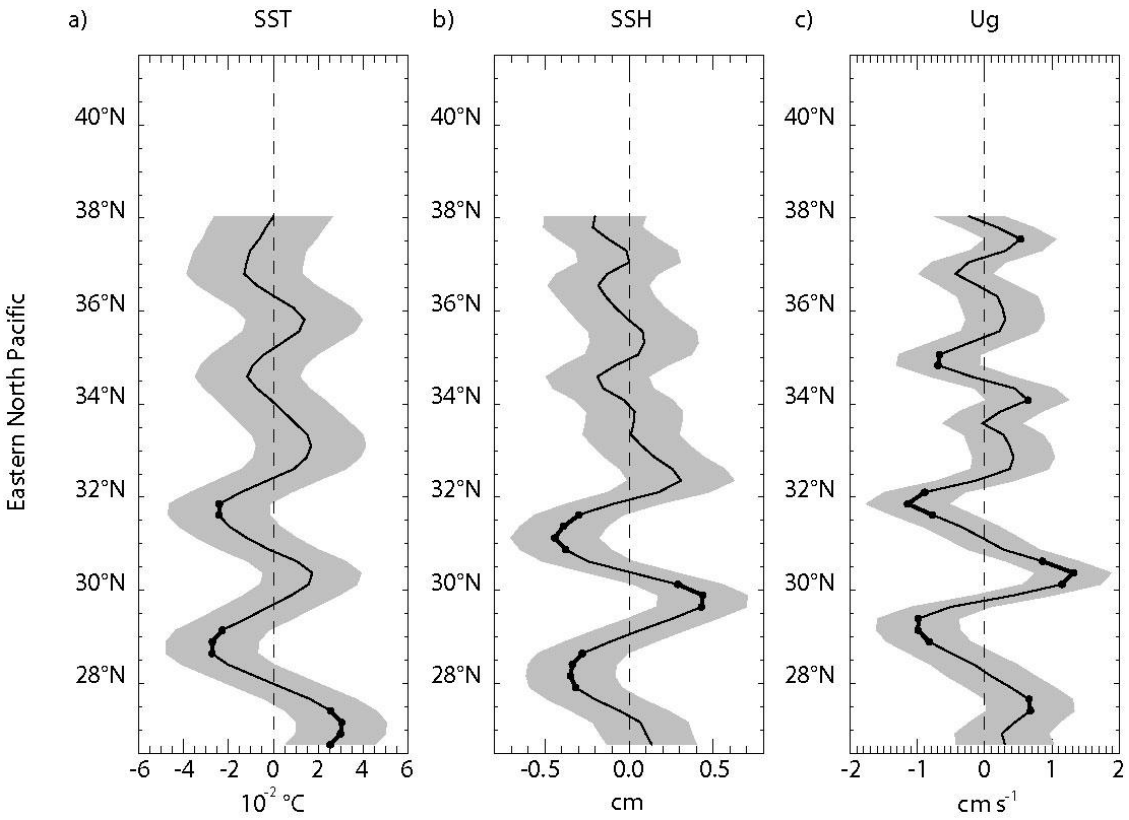

Figure S3. Cross-striation profiles of spatially high-pass filtered (**a**) AMSR-2 SST (10^{-2} °C), SSALTO/DUACS (**b**) SSH (cm) and (**c**) U_g (cm s^{-1}) fields in the ENP, averaged quasi-zonally within the tilted solid box on Figure 2a and temporally over 07/02/12-12/31/18. The shaded areas are for the 90% confidence intervals associated with each profile. The dots joined by the thick lines indicate where confidence intervals do not cross zero.

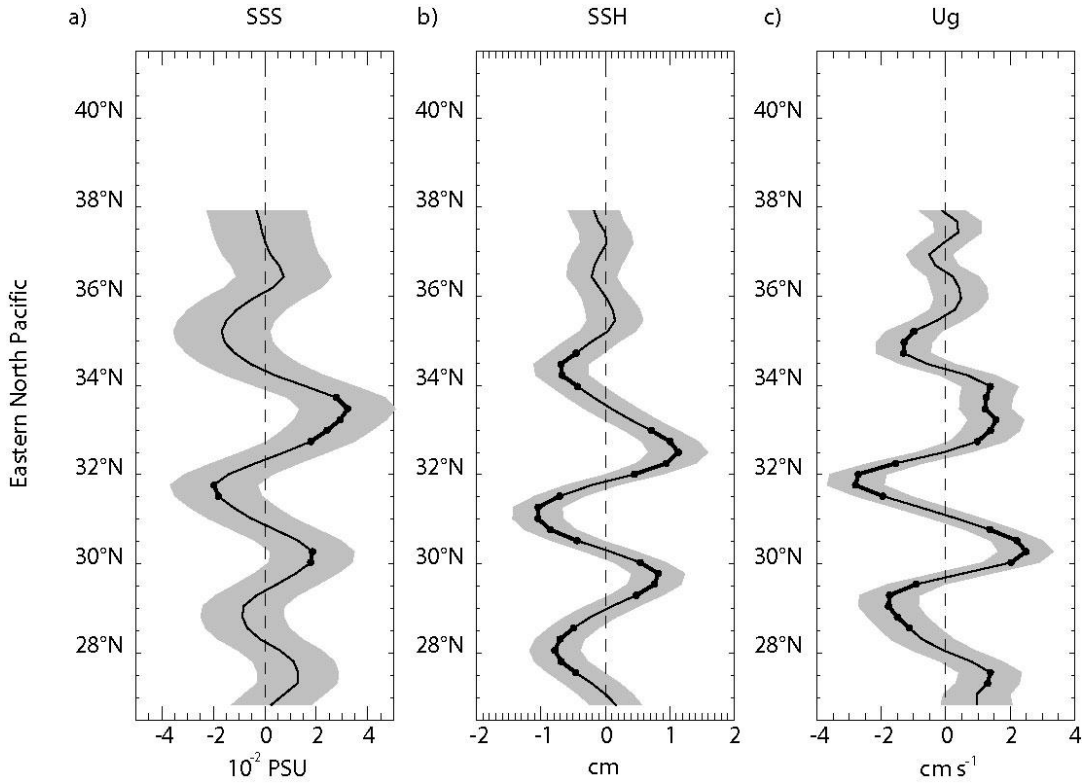

Figure S4. Same as Figure S3, except (**a**) is for SMAP SSS (10^{-2} PSU), and all panels show quasi-zonal averages within the tilted solid box on Figure 2c and over 04/04/15-12/31/18.

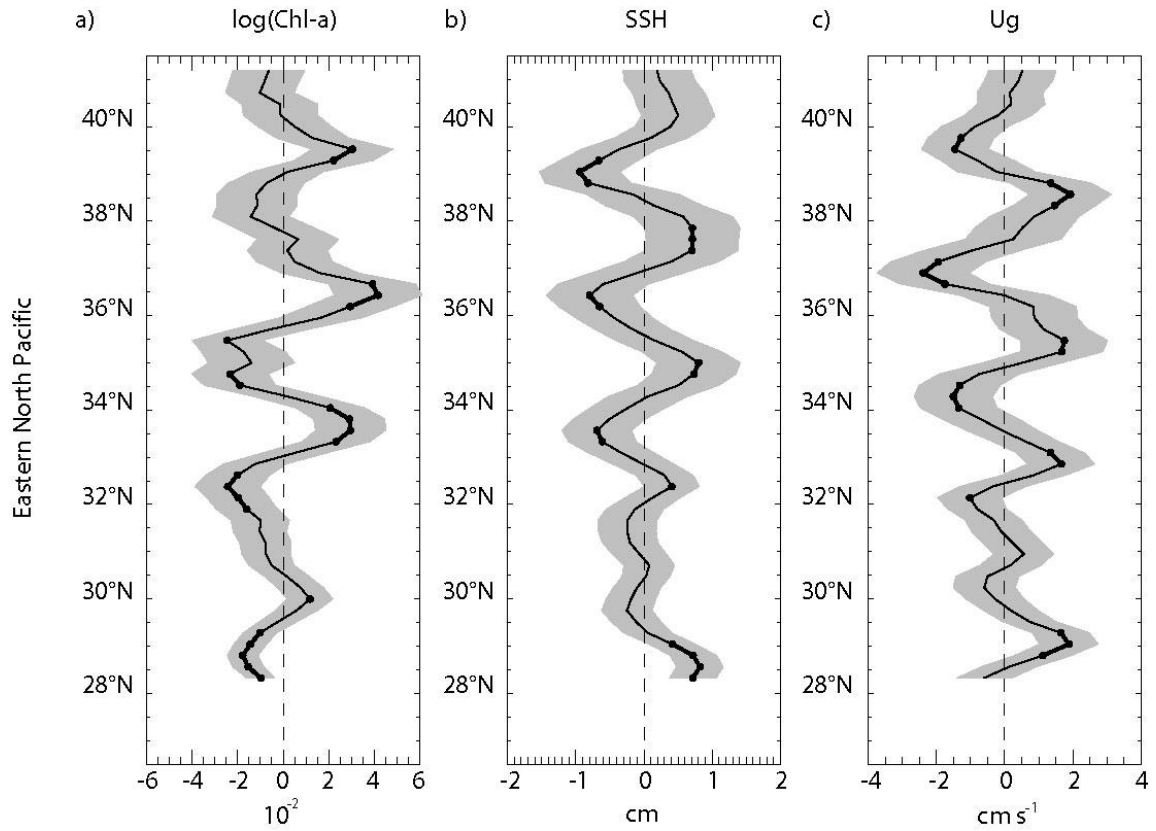

Figure S5. Same as Figure S3, except (**a**) is for GlobColour log(Chl-a) (times 10^{-2}), and all panels show quasi-zonal averages within the tilted solid box on Figure 2e.

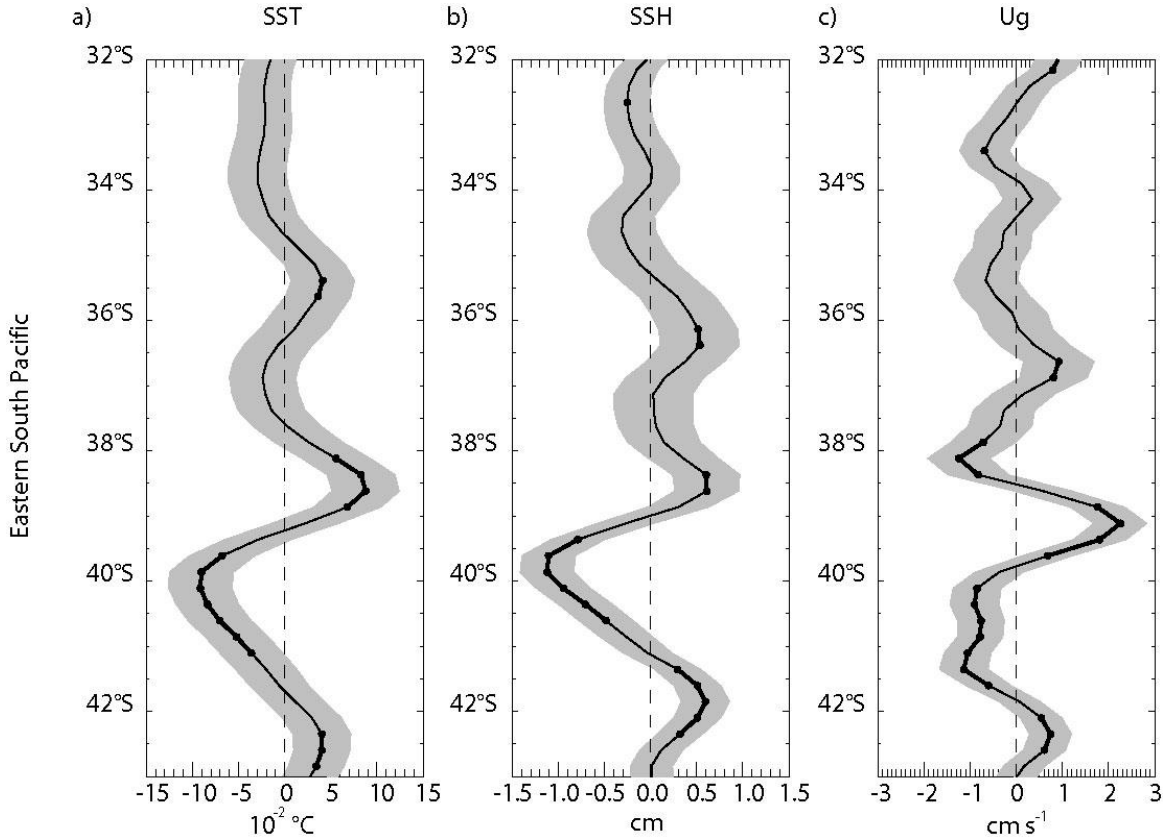

Figure S6. Same as Figure S3, except for the ESP: all panels show quasi-zonal averages within the tilted solid box on Figure 3a.

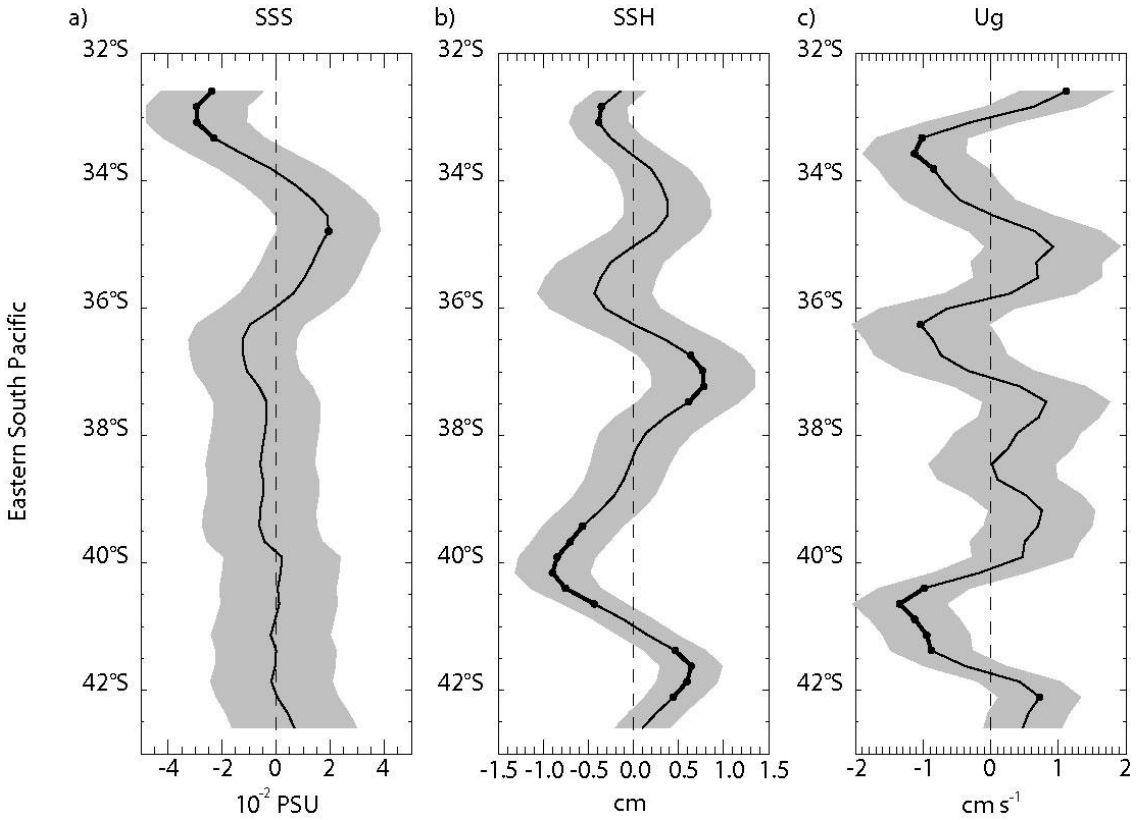

Figure S7. Same as Figure S4, except for the ESP: all panels show quasi-zonal averages within the tilted solid box on Figure 3c.

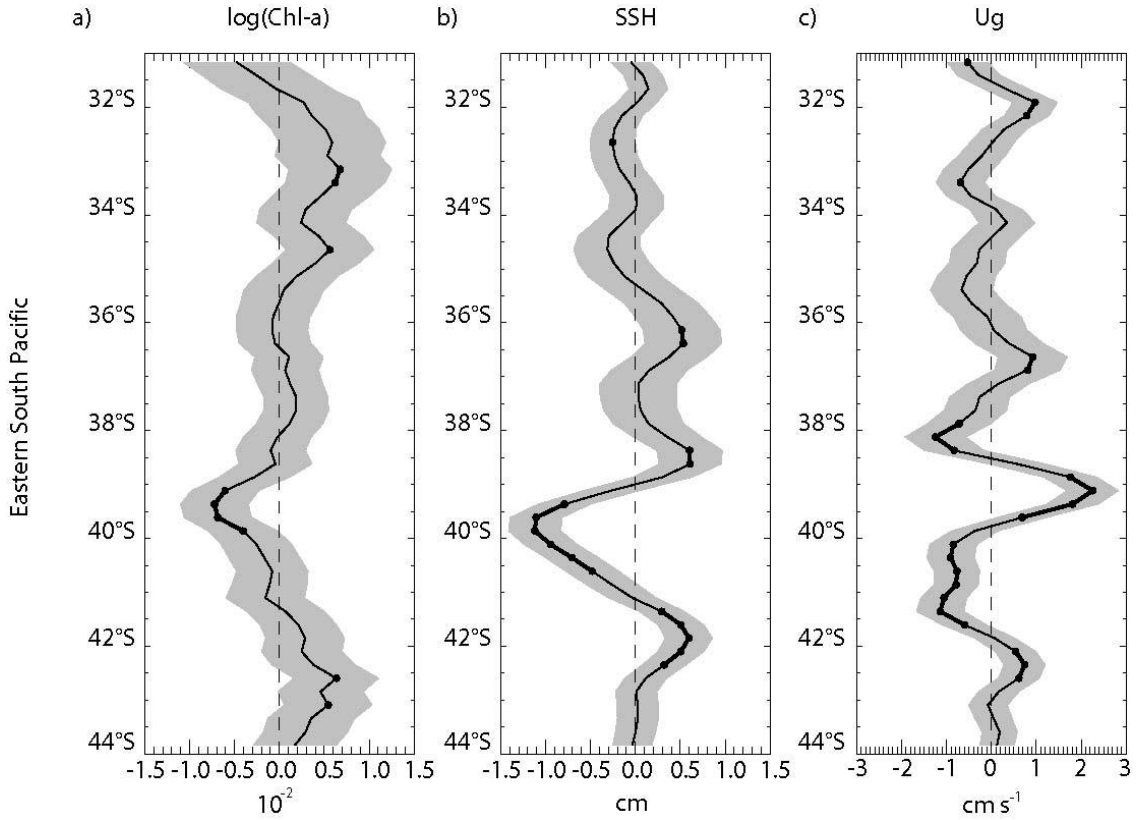

Figure S8. Same as Figure S5, except for the ESP: all panels show quasi-zonal averages within the tilted solid box on Figure 3e.

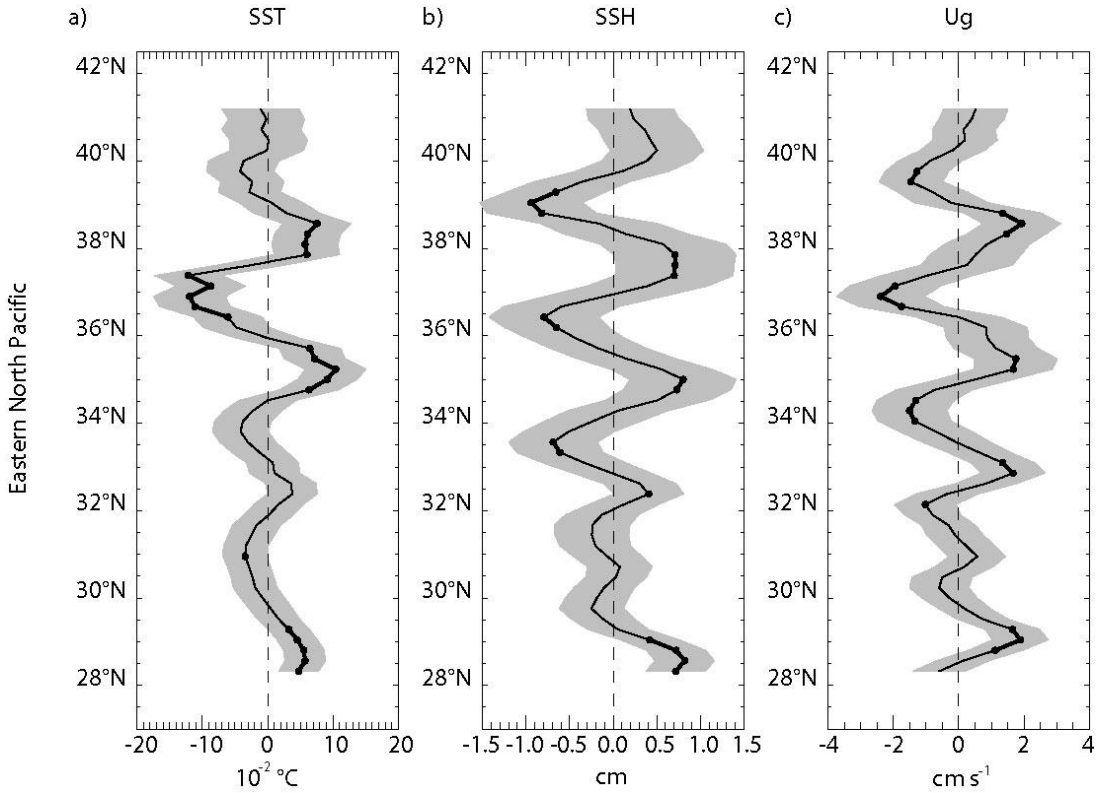

Figure S9. Same as Figure S3, except for the ENP coastal transition zone: all panels show quasi-zonal averages within the tilted solid box on Figure 2e.

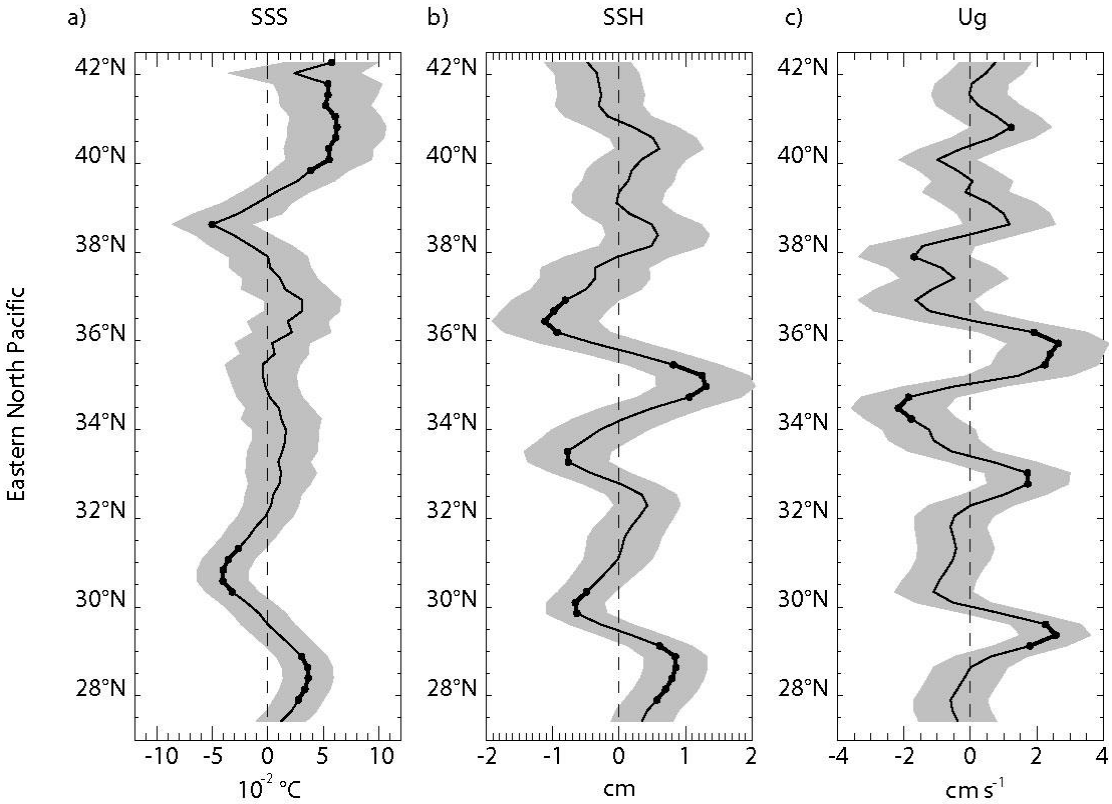

Figure S10. Same as Figure S4, except for the ENP coastal transition zone: all panels show quasi-zonal averages within the tilted solid box on Figure 2e.

Table S1. Results of the MonteCarlo analysis for the correlation coefficients shown on Figures 6a-c : 2.5th/97.5th percentile values obtained from the 1000 iterations as described in Section 2.2. The actual correlation coefficients are repeated here in brackets, with stars (*) indicating values located outside the range obtained from the MonteCarlo analysis, i.e. statistically significant at the 5 % level.

Correlated Variables	SSH	U_g
SST	−0.76 / +0.75 (+0.88*)	−0.68 / +0.67 (+0.81*)
SSS	−0.78 / +0.80 (+0.91*)	−0.77 / +0.78 (+0.82*)
log(Chl-a)	−0.64 / +0.62 (−0.74*)	−0.62 / +0.60 (−0.79*)

Table S2. Results of the MonteCarlo analysis for the correlation coefficients shown on Figures 6d-f.

Correlated Variables	SSH	U_g
SST	−0.62 / +0.62 (+0.77*)	−0.50 / +0.51 (+0.74*)
SSS	−0.67 / +0.70 (+0.20)	−0.56 / +0.58 (+0.34)
log(Chl-a)	−0.41 / +0.45 (+0.36)	−0.32 / +0.33 (−0.22)

Table S3. Results of the MonteCarlo analysis for the correlation coefficients between cross-striation profiles of $\overline{F_H}$ on the one hand, $-\overline{U_{\mathrm{aH}}}\partial\,\overline{F_L}/\partial\,x_a$ or $-\overline{V_{\mathrm{cL}}}\partial\,\overline{F_H}/\partial\,y_c$ on the other hand, as shown on Figures 8b,c for SST and on Figures 9b,c for SSS : 2.5$^{\mathrm{th}}$/97.5$^{\mathrm{th}}$ percentile values obtained from the 1000 iterations as described in Section 2.2. The actual maximum lag-correlation coefficients are indicated in brackets, with stars (*) indicating values located outside the range obtained from the MonteCarlo analysis, i.e. statistically significant at the 5 % level.

Correlated Variables	$-\overline{U_{\mathrm{aH}}}\partial\,\overline{SST_L}/\partial\,x_a$	$-\overline{V_{\mathrm{cL}}}\partial\,\overline{SST_H}/\partial\,y_c$	$-\overline{U_{\mathrm{aH}}}\partial\,\overline{SSS_L}/\partial\,x_a$	$-\overline{V_{\mathrm{cL}}}\partial\,\overline{SSS_H}/\partial\,y_c$
SST	−0.74 / +0.77 (+0.83*)	−0.71 / +0.70 (−0.84*)	/	/
SSS	/	/	−0.71 / +0.73 (+0.77*)	−0.75 / +0.72 (−0.87*)

Table S4. Results of the MonteCarlo analysis for the correlation coefficients shown on Figure 11.

Correlated Variables	SSH	U_g
SST	−0.64 / +0.65 (+0.75*)	−0.62 / +0.59 (+0.78*)
SSS	−0.42 / +0.42 (+0.35)	−0.35 / +0.33 (+0.20)